Atmos. Chem. Phys. Discuss., https://doi.org/10.5194/acp-2017-549
Manuscript under review for journal Atmos. Chem. Phys.
Discussion started: 20 June 2017


Atmospheric Chemistry and Physics Discussions

# Hygroscopicity of organic surrogate compounds from biomass burning and their effect on the efflorescence of ammonium sulfate in mixed aerosol particles

Ting Lei[1,2], Andreas Zuend[4], Yafang Cheng[2,3], Hang Su[2,3], Weigang Wang[1], Maofa Ge[1*]

[1]State Key Laboratory for Structural Chemistry of Unstable and Stable Species, CAS Research/Education Center for Excellence in Molecular Sciences, Institute of Chemistry, Chinese Academy of Sciences, Beijing, 100190, P. R. China

[2]Multiphase Department, Max Planck Institute for Chemistry, Mainz 55128, Germany

[3]Institute for Environmental and Climate Research, Jinan University, Guangzhou, China

[4]Department of Atmospheric and Oceanic Sciences, McGill University, Montreal, Quebec, Canada

*Correspondence to*: M. F. Ge (gemaofa@iccas.ac.cn)

**Abstract:** Hygroscopic growth factors of organic surrogate compounds representing biomass burning and mixed organic-inorganic aerosol particles exhibit variability during dehydration experiments depending on their chemical composition, which we observed using a hygroscopicity tandem differential mobility analyzer (HTDMA). We observed that levoglucosan and humic acid aerosol particles release water slightly in the range of 90 – 5 % relative humidity (RH). 4-Hydroxybenzoic acid aerosol particles, however, remain in the solid state without diameter growth and even slightly shrinking at higher RH compared to the dry size. The measurements were accompanied by RH-dependent thermodynamic equilibrium calculations using the AIOMFAC and the E-AIM models, the ZSR relation, and a fitted hygroscopicity expression. We observed several effects of organic components on the hygroscopicity behavior of mixtures containing ammonium sulfate (AS) in relation to the different mass fractions of organic compounds: (1) a shift of efflorescence relative humidity (ERH) of ammonium sulfate to higher RH due to the presence of 25 wt % levoglucosan in the mixture. (2) There is a distinct efflorescence transition at 25 % RH for mixtures consisting of 25 wt % of 4-hydroxybenzoic acid compared to the ERH at 35 % for organic-free AS particles. (3) There is indication for a liquid-to-solid phase transition of 4-hydroxybenzoic acid in the mixed particles during dehydration. (4) A humic acid component shows no significant effect on the efflorescence of AS in mixed aerosol particles. In addition, relatively good



measurement-model agreement in the case of the AIOMFAC and E-AIM models is mainly due to composition-dependent consideration of crystallization of AS in the model prediction. The use of the ZSR relation leads to good agreement with measured diameter growth factors of aerosol particles containing humic acid and ammonium sulfate. A similarity of the hygroscopicity parameter $\kappa$ for organic surrogate compounds mixed with ammonium sulfate for different mass fractions during the different seasonal periods in the Amazon is observed. The RH-dependent hygroscopicity parameter $\kappa$ measured at sub-saturated is consistent with kappa values for observations in the central Amazon Basin at the same environment, which suggests the similar O: C ratios and ammonium sulfate mass fraction in the laboratory and field observation conditions.

## Introduction

It is well established that biomass burning, as an important source of atmospheric aerosol particles, has a wide range of climate effects that can be classified into direct radiative effects through light-absorbing carbon aerosol particles and indirect effects by impact on cloud condensation nuclei and cloud microphysics (Andreae and Gelencsér, 2006; Moosmüller et al., 2009; Hecobian et al., 2010; Rizzo et al., 2011; Rose et al., 2011; Cheng et al., 2012; Engelhart et al., 2012; Lack et al., 2012; Jacobson, 2014; Liu et al., 2014; Saleh et al., 2013, 2014). Atmospheric light-absorbing particles that arise from biomass burning play an important role as a driver of global warming (Favez et al., 2009; Hegg et al., 2010; Lack et al., 2012; Feng et al., 2013; Laborde et al., 2013; Srinivas and Sarin, 2013). According to the IPCC report (Boucher and David, 2013), the climate forcing of black carbon aerosol particles may rival that of methane, with a present-day global warming effect of up to 0.3–0.4 °C (Wang et al., 2014). Also, certain types of aerosol particles emitted by biomass burning, when immersed into cloud droplets, absorb solar radiation and facilitate water evaporation and cloud dispersion, which indicates an additional indirect aerosol effect that counteracts the cooling effect of cloud droplets nucleated by aerosols (Powelson et al., 2014). Therefore, a better understanding of the influence of aerosol particles from biomass burning on cloud formation, precipitation, and Earth's radiative budget is required to comprehend biomass burning aerosol properties and behavior.

The understanding of aerosol-cloud-climate impact of a vast range of biomass burning derived organic



compounds, however, is rather limited due to the complexity of biomass burning emissions, gas- and aerosol-phase processing and the restricted availability of field measurements (Pratt et al., 2011; Lei et al., 2014; Paglione et al., 2014; Srinivas and Sarin, 2014; Zhong and Jang, 2014; Ciarelli et al., 2015; Arnold et al., 2015; Lawson et al., 2015; Gilman et al., 2015). Moreover, biomass burning particles are often mixtures of water-soluble organic carbon, black carbon, varying amounts of inorganic components, and water insoluble inclusions, such as mineral dust or poorly soluble organics (Väkevä et al., 2002; Sadezky et al., 2005; Saarnio et al., 2010). An appreciable amount of organic compounds affect the physicochemical properties of aerosols, such as hygroscopicity, liquid-solid and liquid-liquid phase transitions, and chemical reactivity in liquid phases and/or on particle surfaces (Shiraiwa et al., 2013). For example, equilibrium between the variable environmental water vapor mixing ratio and aerosol particles may lead to substantial changes in particle size, and chemical composition, all of which can influence light absorption and scattering (Seinfeld and Pandis, 2006; Zhang et al., 2016). RH-dependent transitions between solid and liquid (aqueous) phases are also important in determining optical properties (Martin et al., 2013; Wang et al., 2010; Kim et al., 2016; Wu et al., Denjean et al., 2015; 2016; Hodas et al., 2015; Atkinson et al., 2015). Studies have shown that water-soluble organic matter from biomass burning (approximately 70 % of total organic matter) can significantly suppress, enhance or have no effect on the deliquescence (e.g. the RH at which deliquescence occurs at a certain temperature, the DRH) and efflorescence process (e.g. the efflorescence RH, ERH) of present inorganic electrolytes. The effect depends predominantly on the type of organics, mass fraction of organics relative to inorganic, and particle size (You and Bertram, 2014; Zawadowicz et al., 2015; Hodas et al., 2015; Gupta et al., 2015). Whole particles, individual phases within particles, or specific chemical compounds can undergo a range of phase transitions including crystallization/efflorescence, dissolution/deliquescence, and liquid-liquid phase separation as the relative humidity varies in the atmosphere. A number of laboratory studies have focused on liquid-liquid phase separations within particles consisting of inorganic and organics fractions (Svenningsson et al., 2006; Carrico et al., 2008; Dusek et al., 2011; Hodas et al., 2015). For example, studies about liquid-liquid separation occurring in mixed organic-inorganic aerosols were performed by Song et al. (2012, 2013) and You et al. (2013) using Raman and optical microscopy, establishing that liquid-liquid phase separation occurs typically in mixed organics + ammonium sulfate particles with an average elemental oxygen-to-carbon (O:C) ratio of the organic fraction of less than 0.6 and in some cases for $0.6 < O:C < 0.8$. You et al. (2013) further found that for O:C between 0.5 and 0.8, the occurrence of



liquid-liquid phase separation at moderate to high RH depends on the types of inorganic salts present (i.e., the effective strength of the salting-out effect), e.g., $(NH_4)_2SO_4 \geq NH_4HSO_4 \geq NaCl \geq NH_4NO_3$. Recently, the effect of a potential size-dependent morphology and dependence of the phase separation mechanism on the organic/inorganic mass ratio in mixed aerosol was studied for mixtures of poly-(ethylene glycol)-400 + ammonium sulfate using cryogenic-transmission electron microscopy (Altaf et al., 2016). Therefore, many independent studies suggest that the occurrence of solid-liquid and/or liquid-liquid phase separations, as well as related (temperature-dependent) RH levels of phase transitions (DRH, ERH, SRH), depend on the relative amounts of organic and inorganic aerosols components and their non-ideal mixing behavior.

The expected physical state and morphology of aerosol particles containing mixtures of a wide range of organics and inorganic salts/acids can, in principle, be predicted by a selection of specialized thermodynamic equilibrium models. Such models include the Extended Aerosol Inorganic Model (E-AIM) (Clegg and Seinfeld, 1998, 2006; available online: http://www.aim.env.uea.ac.uk/aim/aim.php), the Aerosol Diameter Dependent Equilibrium Model (ADDEM) (Topping et al., 2004), the UNIversal Quasichemical Functional Group Activity Coefficients model (UNIFAC) (Fredenslund et al.,1975; Hansen et al., 1991), and the Aerosol Inorganic-Organic Mixtures Functional croups Activity Coefficients model (AIOMFAC) (Zuend et al., 2008, 2011, 2012). These models have all been used to predict atmospheric aerosol thermodynamic equilibrium for a variety of inorganic and organic systems, yet not all of them can be used to compute non-ideal mixing in organic-inorganic systems. AIOMFAC has been used to predict the distribution of components in multiple phases in a range of mixed organic-inorganic systems and demonstrated its broad applicability in predicting liquid-liquid phase separation in such mixtures (Zuend et al., 2010; Song et al., 2012; Zuend and Seinfeld, 2012; Shiraiwa et al., 2013; Renbaum-Woff et al., 2016; Rastak et al., 2017).

Several previous experimental studies using the HTDMA technique (e.g. Zardini et al., 2008; Lei et al.2014) show that the deliquescence of inorganic compounds is affected by the presence of organic components, which manifests itself in a shift in the DRH of a salt compared to the corresponding organic-free system. For instance, a clear shift of ammonium sulfate DRH was observed in the case of the levoglucosan + ammonium sulfate system (Lei et al., 2014). Here we focus on investigating the morphology, hygroscopicity and phase transitions of relevant organic compounds found in biomass



116 burning aerosol during the dehydration/dehumidification process. Moreover, we study how the presence
117 of organic compounds affects the water loss behavior of mixed organic-inorganic aerosols with
118 ammonium sulfate (AS) in the supersaturated state as well as after efflorescence of AS. In addition, we
119 compare the measured hygroscopicity behavior of mixed aerosol particles with predictions from the
120 Zdanovskii–Stokes–Robinson (ZSR) mixing rule, the E-AIM model and the AIOMFAC model.

121

122 **2 Methods**

123 **2.1 Aerosol system**

124 Three organic compounds, levoglucosan, 4-hydroxybenozic acid and humic acid, were chosen to
125 systematically study the influence of organic surrogate present in biomass burning on the water uptake
126 and evaporation of pure organic and mixed organic-AS-containing aerosol particles. Here we focus on
127 the characterization of hygroscopic growth factors as well as solid-liquid and liquid-liquid phase
128 transitions during the humidification conditions. The chemical substances and their physical properties
129 are characterized in Table 1. All of the experimental solutions were prepared by dissolving in Milli-Q
130 water (resistivity ≥ 18.2 MΩ) and the experiments were conducted at room temperature (~298 K). For
131 the mixtures of ammonium sulfate and organic surrogates the different mass ratios of AS:organic
132 considered are 3:1, 1:1 1:3. The chemical compositions of biomass-burning model mixtures are
133 introduced in Table 2.

134 **2.2 Instrument design**

135 Figure 1 shows the setup of the HTDMA instrument. Poly-dispersed sub-micrometer aerosol particles
136 are generated by atomizing (MSP 1500, MSP) a 0.05 weight % aqueous solution consisting of different
137 mass fractions of inorganic, and organic components, assuming that the composition of the formed
138 aerosol particles is initially the same as that of the solution used in the atomizer. Aerosol particles from
139 an atomizer are routed though homemade silica diffusion dryers and then they pass a Nafion gas dryer
140 (Perma Pure Inc., USA). After aerosol particles were dried to below 5 % RH (RH set point 1, RH1), they
141 are directed to the impactor; those aerosols with diameter less than 1 μm are allowed to pass it and
142 subsequently pass through a $^{85}$Kr electric charger to reach a near-Boltzmann distribution of charges (Liu



et al., 1985). After charging, the aerosol particles enter the first differential mobility analyzer (DMA1) at a sheath flow to aerosol flow ratio of 4:0.3. The sheath flow is circulated by the diaphragm pump in the first loop DMA1 system, and its RH is kept constant at below 5 % RH. The resulting mono-disperse particle population, selected within uncertainty by the DMA1, is then exposed to high RH conditions during which the aerosol flow is humidified to 98 % RH by mixing water through a Nafion membrane humidifier at 30 °C. After passing through a saturator (Perma Pure Inc., USA), the aerosols are dried to a target RH level (RH2) through a series of two single-Nafion tubes (Perma Pure Inc., USA) with RH2 set to a value in the range of 90 % to 5 % RH. Here, a pulse width modulator (PWM) circuit is used to regulate the sheath flow on the basis of a proportional integral derivative (PID) system. When the second Nafion membranes allow for regulating the sheath flow to a desired RH and for controlled flow into the sample stream until the RH2 setting value is equal to the excess RH of sheath flow value (RH3), the mobility diameter of the dehumidified of aerosols at target RH are measured with the second DMA (DMA2, a scanning DMA) coupled with a condensation particle counter CPC (Model 1500, MSP). In addition, the residence time between the humidifier and DMA2 is around 5 s, which is estimated to be sufficient for aerosols to grow /shrink to equilibrium size at a certain RH setpoint. Also, due to recirculation of the sheath flow and the pre-humidification of the aerosol flow, the sheath flow and aerosol sample flow are enabled to rapidly reach the same RH.

### 2.3 Theory and modeling methods

Models were applied to explore the extent to which measured hygroscopic diameter growth factors (HGFs), particle phase states, and phase compositions under sub-saturation conditions can be predicted by thermodynamic equilibrium models. For the AS-containing systems studies, the current thermodynamic equilibrium predictions account for a crystalline AS phase with solid-liquid equilibria prior to the complete deliquescence of AS under hydration conditions. Similarly, the crystallization point followed by a solid-liquid equilibrium of AS needs to be considered to predict the effect of organic components in the mixed particles on the shift/suppression of AS efflorescence during aerosol dehumidification, i.e. referring to processes occurring along the dehydration branch of a HTDMA humidification-dehumidification cycle. The calculation of the ERH of AS in an organic-inorganic solution is thermodynamically related to the solubility limit, but it is not strictly deterministic (unlike the DRH) due to the stochastic nature of nucleation-and-growth of a crystal embryo. The molality of pure

Atmos. Chem. Phys. Discuss., https://doi.org/10.5194/acp-2017-549
Manuscript under review for journal Atmos. Chem. Phys.
Discussion started: 20 June 2017


Atmospheric Chemistry and Physics Discussions

AS at saturation in an aqueous solution is known, e.g. measured by Apelblat (1993) at 298.15 K as $m_{AS}^{(sat)}$ = 5.790 mol/kg, while measurements are most often not available for the solubility limit of AS in aqueous inorganic-organic systems. However, crystalline AS in equilibrium with an aqueous mixture demonstrates a specific molal ion activity product (IAP) in that solution at a given temperature and atmospheric pressure. Here the AIOMFAC-based thermodynamic equilibrium model is used to calculate the DRH and ERH of AS in the multicomponent system based on the known solubility of AS in the organic-free system. Detailed information on the modeling of solid-liquid equilibria and the IAP-based prediction of ERH is given in Zuend et al. (2011) and Hodas et al. (2016). Briefly, the ERH is determined based on the following equations:

$$\mathrm{IAP_{AS}} = \left[a_{NH_4^+}^{(m)}\right]^2 \left[a_{SO_4^{2-}}^{(m)}\right]^1 \quad (1)$$

$$\mathrm{IAP_{AS}^{[crit]}} = c_{\mathrm{AS}} \times \mathrm{IAP_{AS}^{(sat)}} \quad (2)$$

Here $a_{NH_4^+}^{(m)}$ and $a_{SO_4^{2-}}^{(m)}$ are the molal activities of the ammonium and sulfate ions in solution (Zuend et al., 2010). Molality basis is indicated by superscript "($m$)" (which is not a mathematical exponent). $\mathrm{IAP_{AS}^{(sat)}}$ denotes the molal ion activity product of AS at salt saturation computed by the thermodynamic equilibrium model for any aqueous AS system at a certain temperature (here 298.15 K). The calculated molal IAP at saturation of the corresponding binary salt solution is taken as the (known) reference value. The RH at which this $\mathrm{IAP_{AS}^{[sat]}}$ value is reached in certain bulk solution at equilibrium with its environment is the (bulk) DRH of AS. Similarly, the ERH is determined at the point of crystallization by a critical IAP value denoted as $\mathrm{IAP_{AS}^{[crit]}}$ (Hodas et al., 2016), the value of $\mathrm{IAP_{AS}^{[crit]}} > \mathrm{IAP_{AS}^{[sat]}}$ expresses the need for reaching a critical IAP threshold (critical level of AS super-saturation) for highly likely nucleation-and-growth of a new crystalline AS phase. The multiplication factor $c_{\mathrm{AS}}$ is used as a constant coefficient relating the IAP at AS saturation to the one expected at the point of crystallization in aqueous mixed particles. From the comparison of laboratory measurement of ERH for aqueous AS solution to the AIOMFAC-predicted $\mathrm{IAP_{AS}}$ at that RH, the value of $c_{\mathrm{AS}} \approx 30$ was determined; this value is in particular applicable to submicron-sized AS droplets (Zardini et al., 2008; Ciobannu et al., 2010).

An analogous approach is used for the ERH predictions with the E-AIM model, however, since E-AIM provides activity coefficients and activities on mole fraction basis, denoted here by superscript "($x$)"



(rather than molality basis), the value of $c_{AS}^{(x)}$ need to be determined separately for that model. Expressing Eq. (1) by mole-fraction-based activities of $NH_4^+$ and $SO_4^{2-}$ and comparison to the $IAP_{AS}^{(sat,x)}$ and $IAP_{AS}^{(crit,x)}$ computed by E-AIM for AS at the experimental solubility limit and ERH in aqueous AS solutions, a value of $c_{AS}^{(x)} \approx 40$ was determined for the calculation with E-AIM.

As discussed by Lei et al. (2014), predicting of hygroscopic growth factors with E-AIM includes a sophisticated composition-dependent solution density model, which considers the non-ideality effects on apparent molar volumes used for the calculation of the solution density in mixed organic-inorganic systems (Clegg and Wexler, 2011a, b). The AIOMFAC-based model applies a simpler solution density treatment by assuming that the partial molar volumes of solution species are independent of non-ideal interactions, i.e. the mixed solution density is calculated based on linear additivity of pure component solid or liquid volume contributions to obtain the HGF at a given RH. Differences in the density models are expected to lead to relatively small differences in the application to HGF predictions here. Both models include sophisticated sets of equations to compute activity coefficients of all solution components in a thermodynamically consistent manner.

### 2.4 *κ*-Köhler theory and computation of the hygroscopicity parameter *κ*

The hygroscopicity parameter, *κ*, is commonly used to characterize the relative hygroscopicities of individual aerosol particles, known mixtures or complicated atmospheric aerosols (Petters and Kreidenweis, 2007), and to model the composition-dependence of the solution water activity. The saturation ratio, *S*, in the traditional Köhler equation (Eq. 3), over an aqueous droplet is calculated from

$$S = a_w \left( \frac{4\sigma_s M_w}{RT \rho_w D_{wet}} \right) \quad (3)$$

Where $a_w$ is the mole-fraction-based water activity in solution, $M_w$ and $\rho_w$ are the molar mass of water and the density of pure water in the liquid state at temperature $T$, respectively. $D_{wet}$, the "wet" particle diameter at a given RH, is defined by $D_{wet} = HGF \times D_0$. $D_0$ denotes diameter at dry conditions at RH below 5 %. The solution surface tension is denoted by $\sigma_s$. In the "*κ*-Köhler theory", the bulk solution water activity is described by a single parameter *κ*, with the hygroscopic parameter of the overall mixture related to Eq. (3) by

Atmos. Chem. Phys. Discuss., https://doi.org/10.5194/acp-2017-549
Manuscript under review for journal Atmos. Chem. Phys.
Discussion started: 20 June 2017


Atmospheric Chemistry and Physics Discussions

$$\kappa_{HGF} = 1 - HGF^3 + \frac{HGF^3 - 1}{S} \exp\left[\frac{4\sigma M_w}{RT\rho_w D_{wet}}\right] \quad (4)$$

This expression describes effective values of $\kappa_{HGF}$ as a function of droplet diameter and *HGF* at a certain saturation ratio. In turn, known (measured) solution $\kappa_{HGF}$ values or component-specific $\kappa_i$ values can be used to parameterize or predict the *HGF* curve of a mixture (Petters and Kreidenweis, 2007).

### 2.5 GF data fit

As described by Dick et al. (2001), the relationship between measured hygroscopic growth factors and water activity can alternatively be parameterized by the following expression:

$$HGF = \left[1 + (c_1 + c_2 \times a_w + c_3 \times a_w^2)\frac{a_w}{1 - a_w}\right]^{\frac{1}{3}} \quad (5)$$

By substitution of Eq. (3) for $a_w$ in Eq. (5) and a fit to the measured HGF the three adjustable coefficients $c_1$, $c_2$, $c_3$ of Eq. (5) were determined. The coefficient values are given in Table 3 for the different organic compounds considered.

### 2.6 GF prediction by ZSR

The Zdanovskii-Stokes-Robinson mixing rule is widely used to approximate the water uptake of mixed systems by assuming additivity of the water uptake of each individual component in the mixed particles at a given RH (e.g., Malm and Kreidenweis, 1997). $HGF_{mix}$ is based on the $HGF_j$ of pure components $j$ and their corresponding volume fraction, $\varepsilon_j$ in the mixed particles.

$$HGF_{mix} = \left[\sum_j \varepsilon_j \left(HGF_j\right)^3\right]^{\frac{1}{3}} \quad (6)$$

## 3. Results and discussion

### 3.1 GF of single compounds systems

Figure 2a shows the measured diameter growth factors of AS particles as a function of RH for both humidification and dehumidification conditions. The measured ERH of 100 nm AS particles is

Atmos. Chem. Phys. Discuss., https://doi.org/10.5194/acp-2017-549
Manuscript under review for journal Atmos. Chem. Phys.
Discussion started: 20 June 2017


Atmospheric Chemistry and Physics Discussions

248 approximately 35 % RH at 298.15 K. The models predicted GF and predicted solid-liquid phase transition
249 of AS are in relatively good agreement with the experimental data and, in particular, the efflorescence
250 (crystallization) of AS is captured by the AIOMFAC and E-AIM models. The good model-measurement
251 agreement for the ERH is of course expected, since the aqueous AS system serves as the reference system
252 for determining the value pairs of $IAP_{AS}^{(sat)}$ and $c_{AS}$ on molality and mole fraction basis for use with
253 AIOMFAC and E-AIM, respectively (section 2.3). An ERH of 31 % to 40 % RH was reported by other
254 groups for a range of particle sizes and experimental techniques (Zardini et al., 2008; Ciobanu et al.,
255 2010). There are several factors that contributed to the variability of reported ERH values, such as
256 particles size, temperature, solution impurities and the stochastic nature of the homogeneous or
257 heterogeneous nucleation of a crystalline phase near ERH (Ciobanu et al., 2010).

258 In Fig. 2b, upon dehydration, no efflorescence of the levoglucosan aerosol particles is observed even
259 at RH below 10 %. The agreement of the HGF between the hydration and dehydration processes
260 demonstrates that these particles equilibrate with the surrounding water vapor under these moisture
261 conditions. For example, the measured diameter growth factors of levoglucosan particles at 80, 60, and
262 30 % RH are 1.19, 1.09, 1.03, respectively, which are similar to results obtained for the hydration process
263 of such particles. Levoglucosan has a DRH of ~80 % to 83 % (for a bulk system) at 293 to 298 K
264 (Mochida and Kawamura, 2004; Zamora et al., 2011). The similarity of diameter growth factors under
265 both and hydration and dehydration conditions even below the DRH of levoglucosan is explained by the
266 lack of levoglucosan crystallization upon drying and the presence of a metastable supersaturated aqueous
267 levoglucosan solution in the hydration and dehydration modes for experiments initiated with liquid
268 solution droplets (Mochida and Kawamura, 2004; Svenningsson et al., 2006). A possible reason for a
269 persistent metastable supersaturated solution states is that levoglucosan particles remain liquid (possibly
270 a viscous liquid state) upon drying to below 5 % RH, which was also observed previously (Mochida and
271 Kawamura, 2004), indicating a very low ERH of less than 4 %. Also, the measured diameter growth
272 factors of levoglucosan particles are in good agreement with these estimated from the standard UNIFAC
273 model within the E-AIM model and the AIOMFAC model, within experimental uncertainty. However,
274 the molecular structure of levoglucosan with several polar functional groups in close vicinity may
275 account for a small deviation between models and measured *HGFs* at RH below 70 %, because
276 intramolecular interactions are not fully considered by these models.



The measured diameter growth factors of 4-hydroxybenzoic acid particles shown in Fig. 2c demonstrate untypical increase in diameter of 4-hydroxybenzoic acid particles during dehumidification from 90 to 10 % RH, which is consistent with previous diameter growth factor for a few solid particles (Mochida and Kawamura, 2004). The organic particles measured are likely always in the effloresced, i.e. crystalline state apparently even at high RH. The apparent increase in diameter during dehumidification may be explained by particle shape restructuring, since the (poly)-crystalline particles are likely non-spherical at dry conditions, but may become more sphere-like in shape when exposed to higher RH (Mikhailov et al., 2004). Also, no ERH of 4-hydroxybenzoic acid in the dehydration mode is observed in the experiments, the likely reason is that the highest RH reached in the setup, which is 98 % in the supersaturated humidifier, may already be below the ERH of 4-hydroxybenzoic acid, which is above 98 % RH (Mochida and Kawamura, 2004). As discussed previously by Lei et al. (2014), our HTDMA experiments are carried out such that RH = 98 % is reached initially before dehumidification to a series of relative humidities at set point RH2 (90 % – 5 % RH), the crystallization of the organic, however, could occur at above 90 % RH. In addition, deviations between measurements and model prediction are obvious in Fig. 2c. The observations therefore suggest that 4-hydroxybenzoic acid particles are solid at 90 % RH, and remain in the solid phase state during dehumidification in the range from 90 to 5 % RH. In contrast, the thermodynamic equilibrium models calculations were performed under the assumption that the organic compound remains in the liquid state over the entire RH range. Therefore, it is no surprise that the model-predicted curves deviate from the experimental hygroscopic behavior of 4-hydroxybenzoic acid particles.

The measured HGF curves of humic acid aerosol particles during dehumidification and humidification measurements do not agree very well within experimental uncertainty, in particular above 70 % RH. For instance, the growth factor of humic acid aerosol particles at 80 % RH is 1.2 according to the dehumidification measurement, which is higher than that of humic acid particles in the humidification mode at the same RH. Humic acid aerosol particles shrink continuously due to loss of water content in the range from 90 % to 10 % RH. However, to our knowledge, no results of the hygroscopic growth factor of humic acid aerosol particles in the dehydration mode were reported in previous studies, while several groups studied the hygroscopic growth behavior of humic acid aerosol particles from low to high RH, i.e. during humidification. For example, leonardite standard humic acid particles take up water



306 continuously from low to high RH, which was reported by Brooks et al., (2004). In addition, the
307 experimental growth factor of humic acid aerosol particles during dehumidification can be represented
308 well by fitting Eq. (5) to the measurements. The determined fit parameters are listed in Table 3. The
309 humic acid sample used (Aldrich, 99%) are a mixture of different poly-carboxylic acids of undefined
310 chemical structure. However, specific information on the chemical structure and mixture composition is
311 necessary for corresponding model predictions with AIOMFAC and E-AIM. Therefore, no such model
312 calculations are shown in Fig. 2d.

313 **3.2 GF of mixtures of organic surrogate compounds + ammonium sulfate**

314 Biomass burning aerosol particles are likely mixtures of a diversity of inorganic constituents and organic
315 compounds in the atmosphere. For example, particles may consist of a combination of ammonium sulfate
316 mixed with low- and semi-volatile organics from biomass burning emissions (Lee et al., 2003; Zhang et
317 al., 2007; Pratt and Prather, 2010). Different water solubilities, and hygroscopic behavior of distinct
318 organic compounds may affect the hygroscopic growth factors of mixtures of partially or fully dissolved
319 inorganic and organic components. For example, Bodsworth et al. (2010) studied the effect of different
320 mass fractions of citric acid on the efflorescence properties of mixed citric acid-ammonium sulfate
321 particles at lower temperature and concluded that adding citric acid decreases the ERH of ammonium
322 sulfate in the mixed aerosol particles. These hygroscopic behaviors of mixed aerosol particles, including
323 phase transition in the range from moderate to low RH, are the focus of attention in this study.

324 **3.2.1 Mixed system: levoglucosan + ammonium sulfate**

325 Figure 3 shows measured growth factors of mixed aerosol particles containing levoglucosan +
326 ammonium sulfate with different dry state organic-to-inorganic mass ratios (1:3, 1:1, 3:1) in the RH range
327 from 90 % to 10 %. There is a reduction in the diameter growth factor of aerosol particles containing
328 levoglucosan and AS with increasing levoglucosan mass fraction, as expected from a ZSR-like additivity
329 concept of hygroscopicity. There is a minor shift in the efflorescence point of AS to a higher RH in Fig.
330 3a (ERH of 40 % – 45 %), which suggests a significant influence of levoglucosan on the efflorescence
331 of AS, or its absence (Fig. 3b, c) in the mixed aerosol particles. With a higher mass fraction of
332 levoglucosan, mixtures release water gradually without a clear phase changes in the whole range of RH
333 studied (down to 10 % RH). However, there remains the possibility for efflorescence of AS accompanied



by a small step change in the measured dehydration curve beyond the detection limit of our measurements. The rather high viscosity of solutions containing levoglucosan is expected to increase considerably toward lower RH (Marshall et al., 2016). This increase in viscosity might suppress the crystallization of AS in the mixed systems. Similar observations have been reported for mixtures of AS with citric acid, glutaric acid, adipic acid or octanoic acid with different molar masses of the organic component (Choi and Chan., 2002; Sjogren et al., 2007; Zardini et al., 2008; Ciobanu et al., 2010; Smith et al., 2012; Mikhailov et al., 2013; Hodas et al., 2015; Liu et al., 2015; Jing et al., 2016). For example, in the case of mixtures of ammonium sulfate and citric acid with different organic/inorganic molar ratios (2:1, 1:1), delaying or suppressing AS efflorescence is attributed to the effect of citric acid on the mixed aerosol particle viscosity at moderate and low RH (Zardini et al., 2008).

In addition, the measured diameter growth factors of mixtures of levoglucosan and AS are compared to calculations of hygroscopic growth by the E-AIM and AIOMFAC models. The E-AIM prediction is in relatively good agreement with results from the HTDMA measurement but slightly overestimates the water content of mixtures of aerosol particles before ERH of AS for all of the mixed systems. The liquid-solid phase transition of ammonium sulfate in the mixed particles is considered in the E-AIM assumptions as described in Section 2.3. There is a more distinct shift of ERH of AS with higher mass fractions of levoglucosan. In the case of the AIOMFAC and E-AIM model predictions, it is assumed that the diameter growth factor contribution from AS is zero below the predicted ERH, i,e. there the growth factor deviation from 1.0 is solely due to the organic water uptake. The model prediction shows a slight deviation from the measurements, which may be in part due to (i) model uncertainty in the correct description of the hygroscopicity of levoglucosan, (ii) due to incomplete representation of AS + levoglucosan interactions in aqueous solutions and (iii) in part due to measurement error. Also, in the case of mixtures consisting of AS and levoglucosan with organic-to-inorganic dry mass ratio of 3:1 (75 wt % levoglucosan of dry particle composition), the underestimation of the growth factor by the AIOMFAC model at RH < 35 % in comparison to the measurements is explained in part by the model prediction of AS efflorescence (which seems to be absent in the measurements). However, with decreasing AS mass fraction, the hygroscopic behavior of levoglucosan dominates the diameter growth factors of the mixtures, in relative agreement with the AIOMFAC-modeled “dehydration branch” prediction. Minor differences in the AIOMFAC prediction vs. -measurement for diameter growth factors



of mixed levoglucosan and AS in the RH range of 35 - 25 % here might be attributed to mixture viscosity effects at the higher levoglucosan contents, which may suppress the efflorescence of AS in the mixed systems on experimental timescale or it could simply be due to sufficient miscibility of dissolved AS in the aqueous levoglucosan solution (beyond that predicted by the model), such that a small step-change due to AS efflorescence could be beyond the experimental detection range. As a result, accounting for the effect of the organic components on the diameter growth factors of mixtures within aerosol particles is crucial to model accurately the equilibrium hygroscopic behavior.

### 3.2.2 Mixed system: 4-hydroxybenzoic acid + ammonium sulfate

Mixtures of 4-hydroxybenzoic acid + AS with different organic mass fraction (25, 50, 75 wt %) exhibit a gradual water desorption before the AS fraction of the particle effloresces at a certain RH. With increasing 4-hydroxybenzoic acid mass fraction, no discontinuity step at the corresponding ERH in the dehydration curve of mixtures is observed. This suggests the presence of 4-hydroxybenzoic acid in the liquid state retards or offsets the efflorescence of AS in the mixtures. An interesting, yet contrasting phenomenon was observed for the hydration process of aerosol mixtures containing 4-hydroxybenzoic acid and AS by Lei et al. (2014). For the case of these mixtures during moistening, the hygroscopic behavior is seemingly unaffected by the presence of 4-hydroxybenzoic acid, and the deliquescence point of AS remains at approximately 80 % RH (the value for pure AS particles at 298 K). The DRH and ERH of pure organics and AS in the mixed organic-AS particles are summarized in Table 4, the measurements indicate that 4-hydroxybenzoic acid has a significant effect on the efflorescence of AS when present in sufficient amount. Also, there is a clear reduction in the diameter growth factors prior to crystallization for mixtures with increasing 4-hydroxybenzoic acid mass fraction.

The measurements of mixtures consisting of 4-hydroxybenzoic acid and AS are compared with model predictions based on different assumptions about the phase state of the organic component, since the deviation from measurements might partly be explained by a transition in the physical state of the organic component. The E-AIM model prediction is referring to a system where the mixtures of 4-hydroxybenzoic acid is assumed to be in the liquid state at all RH levels, which the efflorescence of AS is considered. Neglecting the potential efflorescence of the organic component in the dehydration branch makes a systematic offset more obvious prior to the efflorescence of AS. A good E-AIM model-



391 measurement agreement occurs below the predicted ERH of AS for mixed particles. The overestimation
392 of HGFs before the efflorescence of AS is explained by the AIOMFAC model prediction with distinct
393 assumptions about the organic phase state. A possible reason for the departure of model-measurement
394 agreement at RH < 80 % is that there are two liquid-to-solid phase transitions, occurring in the mixed
395 particles: a gradual one for the organic component and a step-like one for AS at lower RH. This
396 phenomenon is shown in the grid square range in Fig. 4 and supported by comparison of the measured
397 HGF data with AIOMFAC-based predictions for two assumptions about the organic phase state,
398 especially in the case of mixtures with 50 and 75 wt-% organic. In the Fig. 4b, good agreement between
399 measurements and the AIOMFAC model prediction with liquid organic assumption is found for RH >
400 65 %, while for RH ≤ 60 % the experimental data agree very well with the dashed red model curve for
401 the case with consideration of a solid organic component. It suggests that crystallization followed by
402 gradually increasing partitioning of organic from the solution to the solid organic phase occurs in the
403 range from 70 % to 60 % RH under conditions of dehumidification. Meanwhile, AS remains dissolved
404 in the supersaturated liquid solution. Similarly, a liquid-to-solid phase transition occurs for the organic:
405 AS mass ratio of 3:1 cases in the range from 80 % to 50 % RH. Interestingly, there is evidence from the
406 comparison of the measured GF and the AIOMFAC predictions that 4-hydroxybenzoic acid remains
407 dissolved in the liquid phase at high RH in the mixed particles. In contrast, in the case of pure 4-
408 hydroxybenzoic acid aerosol particles, particles exposed to initial RH of ≥ 90 % remain in the solid
409 state ( or crystallize at RH > 90 %) in the dehydration mode (Fig. 2c). What factors contribute to keeping
410 the organic in the liquid solution? It is possible that the aerosols generated with those mixed solutions
411 were allowing the 4-hydroxybenzoic acid to fully dissolve as the AS provides substantial particle phase
412 water content (within short time) into which the organic can be dissolved and may then further contribute
413 to water uptake associated with the organic's hygroscopicity (unlike in the case of the pure 4-
414 hydroxybenzoic acid particles). The 4-hydroxybenzoic acid remains dissolved in the mixture, possibly
415 supersaturated with respect to the crystalline organic state (similarly to how AS stays supersaturated at
416 RH below the DRH during drying). We consider this a reasonable explanation for the observed HGF data
417 from the HTDMA in comparison to the different AIOMFAC-based curves.

418 **3.2.3 Mixed system: humic acid + ammonium sulfate**

419 Figure 5 shows that the experimental diameter growth factors of mixtures consisting of humic acid (HA)



and AS with dry mass ratios of 1:3, 1:1 or 3:1 decreases with increasing mass fraction of HA at RH > 35 %. For example, at 35 % RH the measured HGF are 1.1, 1.05, 1.05 for the particles consisting of 25 wt %, 50 wt % and 75 wt % humic acid. In comparison, the diameter growth factor of pure supersaturated AS particles is ~ 1.13 just prior to efflorescence of AS. Humic acid, unlike levoglucosan and 4-hydroxybenzoic acid aerosol particles, has no noticeable effect on the efflorescence point of AS in the mixed aerosol particles. Results of the ZSR model agrees well with measured hygroscopic growth for mixtures within the experimental error. The ZSR curves shown in Fig. 5 are based on the RH-dependent fitted hygroscopic growth factors of humic acid with Eq. (5) and the AIOMFAC predicted diameter growth factors of AS in the dehydration mode. The success of the ZSR mixing rule for this system suggests that interactions of organic molecules with ammonium sulfate ions in aqueous solution will only marginally affect the hygroscopic growth factors of the mixtures containing humic acid and AS. Due to the lack of detailed information about the actual chemical structures of humic acid samples used, it was not possible to perform E-AIM and AIOMFAC model predictions for comparison with the measurement.

### 3.3 Mixtures of biomass burning organic surrogate components with ammonium sulfate

To represent biomass burning organic compounds, we use mixtures of levoglucosan, 4-hydroxybenzoic acid, and humic acid, as a set of surrogate compounds to represent more complex mixtures present in atmospheric biomass burning aerosols containing a variety of neutral compounds, mono/di-carboxylic acids, and polyacids (Liu et al., 2015; Jing et al., 2016). In brief, the water soluble organic compounds (WSOC) observed in the field are often classified into neutral compounds consisting of sugar-like compounds, aromatic acids, and complex poly-carboxylic acids. The reason to study these WSOC is because the mass percentages of organic surrogate compounds vary with different seasons (dry and wet) in the Amazon basin near Rondônia, Brazil (Decesari et al., 2006; Rissler et al., 2006). Hence, it is of significance to explore the dehumidification process of aerosol particles consisting of surrogate organic compounds and ammonium sulfate.

#### 3.3.1 Mixtures system: mix-bio-dry and mix-bio-wet aerosol particles

Figure 6a shows the observed small differences in the hygroscopicity parameter $\kappa$ for mixtures of organic surrogate components and ammonium sulfate representing biomass burning particles during the dry and wet periods in the Amazon, respectively. Hygroscopicity parameter values for bio-mix-dry aerosol



448 particles were determined to be between 0.16 and 0.18 with decreasing RH in the range from 90 % to
449 40 % RH. The $\kappa$ value representing the wet period in the Amazon is shown in Fig. 6b, derived from
450 laboratory HTDMA measurements in the range from 90 % to 40 % RH. In the case of $\kappa$ of organic
451 surrogates mixed with ammonium sulfate, the relevant $\kappa$ value range is ~ 0.12 to 0.15 obtained from 90 %
452 to 40 % RH. The measured $\kappa$ values of the mixtures are compared to field data of HTDMA and CCN
453 measurements conducted at a remote rainforest site in the central Amazon during the dry and wet seasons
454 (Whitehead et al., 2016; Pöhlker et al., 2016), which are consistent with $\kappa$ obtained at similar field sites
455 (within the uncertainty of experiments). The likely reason for a relatively good agreement between the
456 hygroscopicity of the laboratory mixtures and the field data is that the organic mass fractions of the mix-
457 bio-dry and mix-bio-wet mixtures are chosen in our laboratory experiments to be similar to those of the
458 latest field data from Amazon. For example, Pöhlker et al. (2016) obtained the effective hygroscopicity
459 parameters $\kappa$ between 0.3 ± 0.01 and 0.15 ± 0.01 based on the organic mass fraction range from 0.65 to
460 0.97 in the dry season by aerosol chemical speciation monitor (ACSM) and CCN measurements. The
461 predicted $\kappa$ values of the mixtures at various RH levels shown in Fig. 6 (black curves) are obtained by
462 application of Eq. (4) with use of the RH-dependent fitted HGFs of the organic surrogates (Eq. 5), the
463 predicted growth factor of AS by the AIOMFAC model (for the humidification case) and the volume
464 fraction based mixing rule for a mixture's HGF (Eq. 6). For these calculations, a solution surface tension
465 of 0.072 J $m^{-2}$ was assumed. These predictions agree relatively well with the experimental $\kappa_{dry}$ and $\kappa_{wet}$
466 values obtained from the HTDMA over a wide range in RH referring to dehumidification conditions (no
467 solid AS). Furthermore, the combined approach of Eqs. (4-6) allows for a prediction of the change in $\kappa$
468 at high RH towards water vapor super-saturation. A small difference in $\kappa$ between sub- and super-
469 saturated conditions is observed for our mixed systems when comparing the HTDMA data and
470 predictions at 90 % RH with the predictions near 100 % RH and the $\kappa$ values from the CNN field
471 measurements. The difference is more pronounced for the wet season case. Rastak et al. (2017) observed
472 a marked difference in apparent hygroscopicity and related mixture $\kappa$ of the organic aerosols (AS-free)
473 occurring in the case of monoterpene-derived secondary organic aerosol (SOA) for sub- vs. super-satured
474 conditions. A smaller difference was reported for the isoprene-derived SOA (Pajunoja et al., 2015: Rastak
475 et al., 2017), more like the difference observed here for the mixtures containing AS (and therefore having
476 overall higher $\kappa$ values than typical salt-free organic aerosols). Rastak et al. (2017) attribute the distinct
477 difference in $\kappa_{SOA}$ of the monoterpene SOA to the limited mutual solubility of certain SOA components



in water, because a single liquid organic-phase of monoterpene oxidation products is present at RH below 95 %, but over a RH range above 95 %, liquid-liquid phase separation is observed by optical microscopy as well as predicted by the AIOMFAC-based equilibrium model. In the mix-bio-wet and mix-bio-dry cases shown in Fig. 6, the likely reason for the change in characteristic mixture hygroscopicity is not necessarily due to a liquid-liquid phase separation at high RH, but simply because at RH > 95 % the water content of hygroscopic particles increases dramatically with a small increase in RH, leading to the predicted change in the mixtures $\kappa$ parameter that is best representing the hygroscopic growth under such high-RH conditions.

To summarize, there is small difference in hygroscopicity parameters between sub-saturated measurement conditions at 90 % RH in the laboratory with HTDMA and supersaturated conditions using CCN measurements, in agreement with the findings of other studies. At regional scale, in the dry and wet period, the hygroscopic behavior in some extent of the Amazon rainforest is influenced significantly by the biomass burning emissions, which enhances CCN activity and droplet number concentrations in warm clouds in that region and influences the radiation balance and cloud life time (Pöschl et al., 2010). Underestimation of organic surrogate component mass fractions in the mixed particles or organic:sulfate mass ratios may be responsible for the slight differences in the determined $\kappa$ parameters of the laboratory and field measurements.

## 4. Conclusions

A number of field-based hygroscopicity studies about biomass burning aerosol focus on the growth factors of mixtures at high RH (e.g. 90 % RH). However, less attention has been paid to the growth behavior at low to moderate RH, limiting the data base for accurate estimates of particles optical and radiative properties over those lower RH ranges. However, this is a RH range in which water uptake or release behavior demonstrates a considerable variability among different organic-inorganic systems. The occurrence or suppression of a liquid-solid phase transition affects the physicochemical particle properties in a relative narrow RH range, potentially leading to particles of different morphology and physical states, affecting effective particle size and density. In this work, measurements and thermodynamic equilibrium predictions for organic-inorganic aerosols related to components from



biomass burning emissions demonstrate a diversity of hygroscopic growth/shrinking behavior. For example, in the case of aerosol mixtures containing levoglucosan and ammonium sulfate, the presence of levoglucosan may cause the efflorescence of AS to occur at higher RH than in pure aqueous AS particles-or it may completely suppress AS efflorescence, as observed for mixtures with a high levoglucosan mass fraction. The growth curves predicted with an AIOMFAC-based thermodynamic equilibrium model reproduce the observations in most cases reasonably well and we demonstrate the usefulness of predictions with different assumption about the physical state of the organic components for the interpretation of experimental data, such as in the case of mixtures of 4-hydroxybenzoic acid and ammonium sulfate. However, the accurate prediction of AS efflorescence or its suppression in mixed particles is difficult. The E-AIM-predicted growth curves reproduce the measured hygroscopic behavior relatively well for the consideration of the effect of 4-hydroxybenzoic acid on the hygroscopic behavior of mixtures with ammonium sulfate, which leads to suppression of the ammonium sulfate efflorescence. In the case of mixtures of humic acid and ammonium sulfate, continuous water desorption of aerosol particles shows no significant effect on the efflorescence of ammonium sulfate. Also, as expected, there is a clear reduction in diameter growth factor of mixed systems, in comparison with that of pure AS particles. In addition, the small difference of hygroscopicity parameters of mix-bio-dry and mix-bio-wet systems between measured data in the laboratory using HTDMA and the field using CCN activity measurements is due to the similar O:C ratios of organic surrogate compounds and ammonium sulfate mass fractions used in the model mixtures when experimental $\kappa$ data from sub- and super-saturated water vapor conditions are compared.

The range of measurement-model comparisons presented in this study indicate that providing accurate thermodynamic model predictions of the hygroscopic growth behavior of mixed organic-inorganic systems remains a challenging problem. At moderate and low RH, where aerosol solution phases become highly concentrated, step-like or gradual crystallization and related solid-liquid equilibria may occur with high sensitivity to the organic/inorganic mass ratio and the chemical nature of the mixture constituents. To further improve thermodynamic equilibrium models for the prediction of hygroscopicity and phase transitions, controlled laboratory experiments with single solutes and/or with mixed organic-inorganic systems of known phase state will be useful to constrain model parameters. Ideally, such measurements should cover the high, intermediate and low RH ranges under humidification and dehumidification



conditions.

***Acknowledgements.*** This project was supported by the Strategic Priority Research Program (B) of the Chinese Academy of Sciences (Grant No. XDB05010400), the National Key Research and Development Program of China (2016YFC0202202), and the National Natural Science Foundation of China (Contract No. 91544227, 41227805)

**Reference**

Altaf, M. B., Zuend, A., and Freedman, M. A.: Role of nucleation mechanism on the size dependent morphology of organic aerosol, Chemical communications, 52, 9220-9223, 2016.

Andreae, M. O. and Gelencser, A.: Black carbon or brown carbon? The nature of light-absorbing carbonaceous aerosols, Atmospheric Chemistry and Physics, 6, 3131-3148, 2006.

Apelblat, A.: The vapour pressures of saturated aqueous solutions of potassium bromide, ammonium sulfate, copper (II) sulfate, iron (II) sulfate, and manganese (II) dichloride, at temperatures from 283 K to 308 K, The Journal of Chemical Thermodynamics, 25, 1513-1520, 1993.

Arnold, S., Emmons, L., Monks, S., Law, K. S., Ridley, D., Turquety, S., Tilmes, S., Thomas, J. L., Bouarar, I., and Flemming, J.: Biomass burning influence on high-latitude tropospheric ozone and reactive nitrogen in summer 2008: a multi-model analysis based on POLMIP simulations, Atmospheric Chemistry and Physics, 15, 6047-6068, 2015.

Atkinson, D. B., Radney, J. G., Lum, J., Kolesar, K. R., Cziczo, D. J., Pekour, M. S., Zhang, Q., Setyan, A., Zelenyuk, A., and Cappa, C. D.: Aerosol optical hygroscopicity measurements during the 2010 CARES campaign, Atmospheric Chemistry and Physics, 15, 4045-4061, 2015.

Bahadur, R., Praveen, P. S., Xu, Y. Y., and Ramanathan, V.: Solar absorption by elemental and brown carbon determined from spectral observations, Proceedings of the National Academy of Sciences of the United States of America, 109, 17366-17371, 2012.

560 Bodsworth, A., Zobrist, B., and Bertram, A. K.: Inhibition of efflorescence in mixed organic-inorganic
561 particles at temperatures less than 250 K, Physical chemistry chemical physics : PCCP, 12, 12259-12266,
562 2010.

563 Boucher Olivier and David, R.: Clouds and Aerosols, PICC, 2013.

564 Brooks, S. D., DeMott, P. J., and Kreidenweis, S. M.: Water uptake by particles containing humic
565 materials and mixtures of humic materials with ammonium sulfate, Atmos. Environ., 38, 1859-1868,
566 2004.

567 Carrico, C. M., Petters, M. D., Kreidenweis, S. M., Collett, J. L., Engling, G., and Malm, W. C.: Aerosol
568 hygroscopicity and cloud droplet activation of extracts of filters from biomass burning experiments,
569 Journal of Geophysical Research, doi:10.1029/2007JD009274, 2008.

570 Cheng, Y. F., Su, H., Rose, D., Gunthe, S. S., Berghof, M., Wehner, B., Achtert, P., Nowak, A., Takegawa,
571 N., Kondo, Y., Shiraiwa, M., Gong, Y. G., Shao, M., Hu, M., Zhu, T., Zhang, Y. H., Carmichael, G. R.,
572 Wiedensohler, A., Andreae, M. O., and Poschl, U.: Size-resolved measurement of the mixing state of soot
573 in the megacity Beijing, China: diurnal cycle, aging and parameterization, Atmospheric Chemistry and
574 Physics, 12, 4477-4491, 2012.

575 Choi, M. Y. and Chan, C. K.: The effects of organic species on the hygroscopic behaviors of inorganic
576 aerosols, Environmental science & technology, 36, 2422-2428, 2002.

577 Ciarelli, G., Aksoyoglu, S., Crippa, M., Jimenez, J. L., Nemitz, E., Sellegri, K., Äijälä, M., Carbone, S.,
578 Mohr, C., O'Dowd, C., Poulain, L., Baltensperger, U., and Prévôt, A. S. H.: Evaluation of European air
579 quality modelled by CAMx including the volatility basis set scheme, Atmos. Chem. Phys., 16, 10313-
580 10332, 2016.

581 Ciobanu, V. G., Marcolli, C., Krieger, U. K., Zuend, A., and Peter, T.: Efflorescence of ammonium sulfate
582 and coated ammonium sulfate particles: evidence for surface nucleation, The Journal of Physical
583 Chemistry A, 114, 9486-9495, 2010.

584 Clegg, S. L. and Seinfeld, J. H.: Thermodynamic models of aqueous solutions containing inorganic
585 electrolytes and dicarboxylic acids at 298.15 K. 2. Systems including dissociation equilibria, Journal of

586 Physical Chemistry A, 110, 5718-5734, 2006.

587 Clegg, S. L. and Wexler, A. S.: Densities and Apparent Molar Volumes of Atmospherically Important
588 Electrolyte Solutions. 1. The Solutes H2SO4, HNO3, HCl, Na2SO4, NaNO3, NaCl, (NH4)(2)SO4,
589 NH4NO3, and NH4Cl from 0 to 50 degrees C, Including Extrapolations to Very Low Temperature and
590 to the Pure Liquid State, and NaHSO4, NaOH, and NH3 at 25 degrees C, Journal of Physical Chemistry
591 A, 115, 3393-3460, 2011a.

592 Clegg, S. L. and Wexler, A. S.: Densities and apparent molar volumes of atmospherically important
593 electrolyte solutions. 2. The systems $H^{(+)}$-$HSO_4^{(-)}$-$SO_4^{(2-)}$-$H_2O$ from 0 to 3 mol $kg^{(-1)}$ as a function of
594 temperature and $H^{(+)}$-$NH_4^{(+)}$-$HSO_4^{(-)}$-$SO_4^{(2-)}$-$H_2O$ from 0 to 6 mol $kg^{(-1)}$ at 25 degrees C using a Pitzer ion
595 interaction model, and $NH_4HSO_4$.H2O and $(NH_4)_3H(SO_4)_2$-$H_2O$ over the entire concentration range, The
596 journal of physical chemistry. A, 115, 3461-3474, 2011b.

597 Decesari, S., Fuzzi, S., Facchini, M. C., Mircea, M., Emblico, L., Cavalli, F., Maenhaut, W., Chi, X.,
598 Schkolnik, G., Falkovich, A., Rudich, Y., Claeys, M., Pashynska, V., Vas, G., Kourtchev, I., Vermeylen,
599 R., Hoffer, A., Andreae, M. O., Tagliavini, E., Moretti, F., and Artaxo, P.: Characterization of the organic
600 composition of aerosols from Rondonia, Brazil, during the LBA-SMOCC 2002 experiment and its
601 representation through model compounds, Atmospheric Chemistry and Physics, 6, 375-402, 2006.

602 Denjean, C., Formenti, P., Picquet-Varrault, B., Pangui, E., Zapf, P., Katrib, Y., Giorio, C., Tapparo, A.,
603 Monod, A., and Temime-Roussel, B.: Relating hygroscopicity and optical properties to chemical
604 composition and structure of secondary organic aerosol particles generated from the ozonolysis of α-
605 pinene, Atmospheric Chemistry and Physics, 15, 3339-3358, 2015.

606 Dick, W. D., Saxena, P., and McMurry, P. H.: Estimation of water uptake by organic compounds in
607 submicron aerosols measured during the Southeastern Aerosol and Visibility Study, Journal of
608 Geophysical Research-Atmospheres, 105, 1471-1479, 2000.

609 Dusek, U., Frank, G. P., Massling, A., Zeromskiene, K., Iinuma, Y., Schmid, O., Helas, G., Hennig, T.,
610 Wiedensohler, A., and Andreae, M. O.: Water uptake by biomass burning aerosol at sub- and
611 supersaturated conditions: closure studies and implications for the role of organics, Atmospheric
612 Chemistry and Physics, 11, 9519-9532, 2011.

613 Engelhart, G. J., Hennigan, C. J., Miracolo, M. A., Robinson, A. L., and Pandis, S. N.: Cloud
614 condensation nuclei activity of fresh primary and aged biomass burning aerosol, Atmospheric Chemistry
615 and Physics, 12, 7285-7293, 2012.

616 Favez, O., Alfaro, S. C., Sciare, J., Cachier, H., and Abdelwahab, M. M.: Ambient measurements of light-
617 absorption by agricultural waste burning organic aerosols, Journal of Aerosol Science, 40, 613-620, 2009.

618 Feng, Y., Chen, Y., Guo, H., Zhi, G., Xiong, S., Li, J., Sheng, G., and Fu, J.: Characteristics of organic
619 and elemental carbon in PM2.5 samples in Shanghai, China, Atmospheric Research, 92, 434-442, 2009.

620 Gilman, J. B., Lerner, B. M., Kuster, W. C., Goldan, P. D., Warneke, C., Veres, P. R., Roberts, J. M., de
621 Gouw, J. A., Burling, I. R., and Yokelson, R. J.: Biomass burning emissions and potential air quality
622 impacts of volatile organic compounds and other trace gases from fuels common in the US, Atmos. Chem.
623 Phys., 15, 13915-13938, 2015.

624 Gupta, D., Eom, H. J., Cho, H. R., and Ro, C. U.: Hygroscopic behavior of NaCl–MgCl2 mixture
625 particles as nascent sea-spray aerosol surrogates and observation of efflorescence during humidification,
626 Atmos. Chem. Phys., 15, 11273-11290, 2015.

627 Hecobian, A., Zhang, X., Zheng, M., Frank, N., Edgerton, E. S., and Weber, R. J.: Water-Soluble Organic
628 Aerosol material and the light-absorption characteristics of aqueous extracts measured over the
629 Southeastern United States, Atmospheric Chemistry and Physics, 10, 5965-5977, 2010.

630 Hegg, D. A., Warren, S. G., Grenfell, T. C., Doherty, S. J., and Clarke, A. D.: Sources of light-absorbing
631 aerosol in arctic snow and their seasonal variation, Atmospheric Chemistry and Physics, 10, 10923-10938,
632 2010.

633 Hodas, N., Zuend, A., Mui, W., Flagan, R., and Seinfeld, J.: Influence of particle-phase state on the
634 hygroscopic behavior of mixed organic–inorganic aerosols, Atmospheric Chemistry and Physics, 15,
635 5027-5045, 2015.

636 Hodas, N., Zuend, A., Schilling, K., Berkemeier, T., Shiraiwa, M., Flagan, R. C., and Seinfeld, J. H.:
637 Discontinuities in hygroscopic growth below and above water saturation for laboratory surrogates of
638 oligomers in organic atmospheric aerosols, Atmos. Chem. Phys., doi: 10.5194/acp-16-12767-2016, 2016.

639 Jacobson, M. Z.: Effects of biomass burning on climate, accounting for heat and moisture fluxes, black
640 and brown carbon, and cloud absorption effects, Journal of Geophysical Research-Atmospheres, 119,
641 8980-9002, 2014.

642 Jedelsk´y Jiri, L. ı. H. e. y., Pavel Hyn˘cica, and Ivan and Cibulka: Partial molar volumes of organic
643 solutes in water. IV. Benzoic and hydroxybenzoic acids at temperatures from T D 298 K to T D 498 K
644 and pressures up to 30 MPa, J. Chem. Thermodynamics, 32, 11, 2000.

645 Jing, B., Tong, S., Liu, Q., Li, K., Wang, W., Zhang, Y., and Ge, M.: Hygroscopic behavior of
646 multicomponent organic aerosols and their internal mixtures with ammonium sulfate, Atmospheric
647 Chemistry and Physics, 16, 4101-4118, 2016.

648 Kim, J., Ahlm, L., Yli-Juuti, T., Lawler, M., Keskinen, H., Tröstl, J., Schobesberger, S., Duplissy, J.,
649 Amorim, A., Bianchi, F., Donahue, N. M., Flagan, R. C., Hakala, J., Heinritzi, M., Jokinen, T., Kürten,
650 A., Laaksonen, A., Lehtipalo, K., Miettinen, P., Petäjä, T., Rissanen, M. P., Rondo, L., Sengupta, K.,
651 Simon, M., Tomé, A., Williamson, C., Wimmer, D., Winkler, P. M., Ehrhart, S., Ye, P., Kirkby, J., Curtius,
652 J., Baltensperger, U., Kulmala, M., Lehtinen, K. E. J., Smith, J. N., Riipinen, I., and Virtanen, A.:
653 Hygroscopicity of nanoparticles produced from homogeneous nucleation in the CLOUD experiments,
654 Atmos. Chem. Phys., 16, 293-304, 2016.

655 Kiss, G., Tombácz, E., and Hansson, H.-C.: Surface Tension Effects of Humic-Like Substances in the
656 Aqueous Extract of Tropospheric Fine Aerosol, Journal of Atmospheric Chemistry, 50, 279-294, 2005.

657 Konovalov, I. B., Beekmann, M., Berezin, E. V., Petetin, H., Mielonen, T., Kuznetsova, I. N., and Andreae,
658 M. O.: The role of semi-volatile organic compounds in the mesoscale evolution of biomass burning
659 aerosol: a modeling case study of the 2010 mega-fire event in Russia, Atmos. Chem. Phys., 15, 13269-
660 13297, 2015.

661 Laborde, M., Crippa, M., Tritscher, T., Juranyi, Z., Decarlo, P. F., Temime-Roussel, B., Marchand, N.,
662 Eckhardt, S., Stohl, A., Baltensperger, U., Prevot, A. S. H., Weingartner, E., and Gysel, M.: Black carbon
663 physical properties and mixing state in the European megacity Paris, Atmospheric Chemistry and Physics,
664 13, 5831-5856, 2013.

665 Lack, D. A., Bahreni, R., Langridge, J. M., Gilman, J. B., and Middlebrook, A. M.: Brown carbon

absorption linked to organic mass tracers in biomass burning particles, Atmospheric Chemistry and Physics, 13, 2415-2422, 2013.

Lack, D. A., Bahreni, R., Langridge, J. M., Gilman, J. B., and Middlebrook, A. M.: Brown carbon absorption linked to organic mass tracers in biomass burning particles, Atmospheric Chemistry and Physics, 13, 2415-2422, 2013.

Lack, D. A., Langridge, J. M., Bahreini, R., Cappa, C. D., Middlebrook, A. M., and Schwarz, J. P.: Brown carbon and internal mixing in biomass burning particles, Proceedings of the National Academy of Sciences of the United States of America, 109, 14802-14807, 2012.

Lawson, S. J., Keywood, M. D., Galbally, I. E., Gras, J. L., Cainey, J. M., Cope, M. E., Krummel, P. B., Fraser, P. J., Steele, L. P., Bentley, S. T., Meyer, C. P., Ristovski, Z., and Goldstein, A. H.: Biomass burning emissions of trace gases and particles in marine air at Cape Grim, Tasmania, Atmos. Chem. Phys., 15, 13393-13411, 2015.

Lee, Y. N.: Airborne measurement of inorganic ionic components of fine aerosol particles using the particle-into-liquid sampler coupled to ion chromatography technique during ACE-Asia and TRACE-P, Journal of Geophysical Research, doi:10.1029/2002JD003265, 2003.

Lei, T., Zuend, A., Wang, W. G., Zhang, Y. H., and Ge, M. F.: Hygroscopicity of organic compounds from biomass burning and their influence on the water uptake of mixed organic ammonium sulfate aerosols, Atmospheric Chemistry and Physics, 14, 1-20, 2014.

Lienhard, D. M., Bones, D. L., Zuend, A., Krieger, U. K., Reid, J. P., and Peter, T.: Measurements of thermodynamic and optical properties of selected aqueous organic and organic-inorganic mixtures of atmospheric relevance, The journal of physical chemistry. A, 116, 9954-9968, 2012.

Liu, B. Y. H., Pui, D. Y. H., and Rubow, K. L. a. S., W.W.: ELECTROSTATIC EFFECTS IN AEROSOL SAMPLING AND FILTRATION, Arm. occup. Hyg., 29, 251-269, 1985.

Liu, J. M., Scheuer, E., Dibb, J., Ziemba, L. D., Thornhill, K. L., Anderson, B. E., Wisthaler, A., Mikoviny, T., Devi, J. J., Bergin, M., and Weber, R. J.: Brown carbon in the continental troposphere, Geophysical Research Letters, 41, 2191-2195, 2014.

692 Liu, Q., Jing, B., Peng, C., Tong, S., Wang, W., and Ge, M.: Hygroscopicity of internally mixed multi-
693 component aerosol particles of atmospheric relevance, Atmos. Environ., 125, 69-77, 2016.

694 Malm, W. C. and Kreidenweis, S. M.: The effects of models of aerosol hygroscopicity on the
695 apportionment of extinction, Atmos. Environ., 31, 1965-1976, 1997.

696 MAN NIN CHAN, A. K. Y. L., AND and CHAN, C. K.: Responses of Ammonium Sulfate Particles
697 Coated with Glutaric Acid to Cyclic Changes in Relative Humidity: Hygroscopicity and Raman
698 Characterization, Environ.Sci.Technol., 40, 6893-6989, 2006.

699 Man Nin Chan, C. K. C.: Mass transfer effects on the hygroscopic growth of ammonium sulfate particles
700 with a water-insoluble coating, Atmos. Environ., doi: 10.1016/j.atmosenv.2007.01.047, 2007.

701 Marshall, F. H., Miles, R. E. H., Song, Y.-C., Ohm, P. B., Power, R. M., Reid, J. P., and Dutcher, C. S.:
702 Diffusion and reactivity in ultraviscous aerosol and the correlation with particle viscosity, Chemical
703 Science, 7, 1298-1308, 2016.

704 Martin, M., Tritscher, T., Juranyi, Z., Heringa, M. F., Sierau, B., Weingartner, E., Chirico, R., Gysel, M.,
705 Prevot, A. S. H., Baltensperger, U., and Lohmann, U.: Hygroscopic properties of fresh and aged wood
706 burning particles, Journal of Aerosol Science, 56, 15-29, 2013.

707 Mikhailov, E., Vlasenko, S., Rose, D., and Pöschl, U.: Mass-based hygroscopicity parameter interaction
708 model and measurement of atmospheric aerosol water uptake, Atmospheric Chemistry and Physics, 13,
709 717-740, 2013.

710 Mochida, M. and Kawamura, K.: Hygroscopic properties of levoglucosan and related organic compounds
711 characteristic to biomass burning aerosol particles, Journal of Geophysical Research-Atmospheres,
712 doi:10.1029/2004JD004962, 2004.

713 Moosmuller, H., Chakrabarty, R. K., and Arnott, W. P.: Aerosol light absorption and its measurement: A
714 review, Journal of Quantitative Spectroscopy & Radiative Transfer, 110, 844-878, 2009.

715 Paglione, M., Saarikoski, S., Carbone, S., Hillamo, R., Facchini, M. C., Finessi, E., Giulianelli, L.,
716 Carbone, C., Fuzzi, S., Moretti, F., Tagliavini, E., Swietlicki, E., Stenstrom, K. E., Prevot, A. S. H.,
717 Massoli, P., Canaragatna, M., Worsnop, D., and Decesari, S.: Primary and secondary biomass burning

718 aerosols determined by proton nuclear magnetic resonance (H-1-NMR) spectroscopy during the 2008
719 EUCAARI campaign in the Po Valley (Italy), Atmospheric Chemistry and Physics, 14, 5089-5110, 2014.

720 Pajunoja, A, AT Lambe, J Hakala, N Rastak, MJ Cummings, JF Brogan, L Hao, M Paramonov, J
721 Hong, NL Prisle, J Malila, S Romakkaniemi, KEJ Lehtinen, A Laaksonen, M Kulmala, P Massoli, TB
722 Onasch, NM Donahue, I Riipinen, P Davidovits, DR Worsnop, T Petäjä, and A
723 Virtanen (2015), Adsorptive uptake of water by semisolid secondary organic aerosols. Geophys. Res.
724 Lett., 42, 3063–3068. doi: 10.1002/2015GL063142.

725 Petters, M. D. and. Kreidenweis, S. M.: A single parameter representation of hygroscopic growth and
726 cloud condensation nucleus activity, Atmos. Chem. Phys., 7, 1961-1971, 2007.

727 Pöhlker, M. L., Pöhlker, C., Ditas, F., Klimach, T., Hrabe de Angelis, I., Araújo, A., Brito, J., Carbone,
728 S., Cheng, Y., and Chi, X.: Long-term observations of cloud condensation nuclei in the Amazon rain
729 forest–Part 1: Aerosol size distribution, hygroscopicity, and new model parametrizations for CCN
730 prediction, Atmospheric Chemistry and Physics, 16, 15709-15740, 2016.

731 Powelson, M. H., Espelien, B. M., Hawkins, L. N., Galloway, M. M., and De Haan, D. O.: Brown Carbon
732 Formation by Aqueous-Phase Carbonyl Compound Reactions with Amines and Ammonium Sulfate,
733 Environmental Science & Technology, 48, 985-993, 2014.

734 Pratt, K. A., Murphy, S. M., Subramanian, R., DeMott, P. J., Kok, G. L., Campos, T., Rogers, D. C.,
735 Prenni, A. J., Heymsfield, A. J., Seinfeld, J. H., and Prather, K. A.: Flight-based chemical characterization
736 of biomass burning aerosols within two prescribed burn smoke plumes, Atmospheric Chemistry and
737 Physics, 11, 12549-12565, 2011.

738 Pratt, K. A. and Prather, K. A.: Aircraft measurements of vertical profiles of aerosol mixing states, Journal
739 of Geophysical Research, doi:10.1029/2009JD013150, 2010.

740 Rastak, N., Pajunoja, A., Acosta Navarro, J. C., Ma, J., Song, M., Partridge, D. G., Kirkevåg, A., Leong,
741 Y., Hu, W. W., Taylor, N. F., Lambe, A., Cerully, K., Bougiatioti, A., Liu, P., Krejci, R., Petäjä, T., Percival,
742 C., Davidovits, P., Worsnop, D. R., Ekman, A. M. L., Nenes, A., Martin, S., Jimenez, J. L., Collins, D.
743 R., Topping, D. O., Bertram, A. K., Zuend, A., Virtanen, A., and Riipinen, I.: Microphysical explanation
744 of the RH-dependent water affinity of biogenic organic aerosol and its importance for climate,

745 Geophysical Research Letters, doi: 10.1002/2017GL073056. 2017.

746 Renbaum-Wolff, L., Song, M., Marcolli, C., Zhang, Y., Liu, P. F., Grayson, J. W., Geiger, F. M., Martin,
747 S. T., and Bertram, A. K.: Observations and implications of liquid–liquid phase separation at high relative
748 humidities in secondary organic material produced by α-pinene ozonolysis without inorganic salts,
749 Atmos. Chem. Phys., 16, 7969-7979, 2016.

750 Rissler, J., Vestin, A., Swietlicki, E., Fisch, G., Zhou, J., Artaxo, P., and Andreae, M. O.: Size distribution
751 and hygroscopic properties of aerosol particles from dry-season biomass burning in Amazonia,
752 Atmospheric Chemistry and Physics, 6, 471-491, 2006.

753 Rizzo, L. V., Correia, A. L., Artaxo, P., Procopio, A. S., and Andreae, M. O.: Spectral dependence of
754 aerosol light absorption over the Amazon Basin, Atmospheric Chemistry and Physics, 11, 8899-8912,
755 2011.

756 Rose, D., Gunthe, S. S., Su, H., Garland, R. M., Yang, H., Berghof, M., Cheng, Y. F., Wehner, B., Achtert,
757 P., Nowak, A., Wiedensohler, A., Takegawa, N., Kondo, Y., Hu, M., Zhang, Y., Andreae, M. O., and
758 Poschl, U.: Cloud condensation nuclei in polluted air and biomass burning smoke near the mega-city
759 Guangzhou, China -Part 2: Size-resolved aerosol chemical composition, diurnal cycles, and externally
760 mixed weakly CCN-active soot particles, Atmospheric Chemistry and Physics, 11, 2817-2836, 2011.

761 Saarnio, K., Aurela, M., Timonen, H., Saarikoski, S., Teinila, K., Makela, T., Sofiev, M., Koskinen, J.,
762 Aalto, P. P., Kulmala, M., Kukkonen, J., and Hillamo, R.: Chemical composition of fine particles in fresh
763 smoke plumes from boreal wild-land fires in Europe, Science of the Total Environment, 408, 2527-2542,
764 2010.

765 Sadezky, A., Muckenhuber, H., Grothe, H., Niessner, R., and Poschl, U.: Raman micro spectroscopy of
766 soot and related carbonaceous materials: Spectral analysis and structural information, Carbon, 43, 1731-
767 1742, 2005.

768 Saleh, R., Hennigan, C. J., McMeeking, G. R., Chuang, W. K., Robinson, E. S., Coe, H., Donahue, N.
769 M., and Robinson, A. L.: Absorptivity of brown carbon in fresh and photo-chemically aged biomass-
770 burning emissions, Atmospheric Chemistry and Physics, 13, 7683-7693, 2013.

771 Saleh, R., Robinson, E. S., Tkacik, D. S., Ahern, A. T., Liu, S., Aiken, A. C., Sullivan, R. C., Presto, A.
772 A., Dubey, M. K., Yokelson, R. J., Donahue, N. M., and Robinson, A. L.: Brownness of organics in
773 aerosols from biomass burning linked to their black carbon content, Nature Geoscience, 7, 647-650, 2014.

774 Seinfeld, J. and Pandis, S.: Atmospheric chemistry and physics. Hoboken. NJ: Wiley, 2006.

775 Shantanu H. Jathar, A. M., Kekkey C. Barsabti, William E. Asher, James F, Pankow and Michael J.
776 Kleeman: Water uptake by organic aerosol and its influence on gas/particle partitioning of secondary
777 organic aerosol in the United States doi: 10.1016/j.atmosenv.2016.01.001, 2016.

778 Shiraiwa, M., Zuend, A., Bertram, A. K., and Seinfeld, J. H.: Gas-particle partitioning of atmospheric
779 aerosols: interplay of physical state, non-ideal mixing and morphology, Physical Chemistry Chemical
780 Physics, 15, 11441-11453, 2013.

781 Sjogren, S., Gysel, M., Weingartner, E., Baltensperger, U., Cubison, M. J., Coe, H., Zardini, A. A.,
782 Marcolli, C., Krieger, U. K., and Peter, T.: Hygroscopic growth and water uptake kinetics of two-phase
783 aerosol particles consisting of ammonium sulfate, adipic and humic acid mixtures, Journal of Aerosol
784 Science, 38, 157-171, 2007.

785 Smith, M. L., Bertram, A. K., and Martin, S. T.: Deliquescence, efflorescence, and phase miscibility of
786 mixed particles of ammonium sulfate and isoprene-derived secondary organic material, Atmospheric
787 Chemistry and Physics, 12, 9613-9628, 2012.

788 Song, M., Marcolli, C., Krieger, U. K., Zuend, A., and Peter, T.: Liquid-liquid phase separation and
789 morphology of internally mixed dicarboxylic acids/ammonium sulfate/water particles, Atmospheric
790 Chemistry and Physics, 12, 2691-2712, 2012.

791 Song, M., Marcolli, C., Krieger, U. K., Zuend, A., and Peter, T.: Liquid-liquid phase separation in aerosol
792 particles: Dependence on O:C, organic functionalities, and compositional complexity, Geophysical
793 Research Letters, 39, doi:10.1029/2012GL052807, 2012.

794 Srinivas, B. and Sarin, M. M.: Brown carbon in atmospheric outflow from the Indo-Gangetic Plain: Mass
795 absorption efficiency and temporal variability, Atmos. Environ., 89, 835-843, 2014.

796 Srinivas, B. and Sarin, M. M.: Light absorbing organic aerosols (brown carbon) over the tropical Indian

797 Ocean: impact of biomass burning emissions, Environmental Research Letters, doi:10.1088/1748-
798 9326/8/4/044042, 2013.

799 Svenningsson, B., Rissler, J., Swietlicki, E., Mircea, M., Bilde, M., Facchini, M. C., Decesari, S., Fuzzi,
800 S., Zhou, J., Monster, J., and Rosenorn, T.: Hygroscopic growth and critical supersaturations for mixed
801 aerosol particles of inorganic and organic compounds of atmospheric relevance, Atmospheric Chemistry
802 and Physics, 6, 1937-1952, 2006.

803 Topping, D., McFiggans, G., and Coe, H.: A curved multi-component aerosol hygroscopicity model
804 framework: Part 1–Inorganic compounds, Atmospheric Chemistry and Physics, 5, 1205-1222, 2005.

805 Tuckermann, R. a. C., H. K.: The surface tension of aqueous solutions of some atmospheric water-soluble
806 organic compounds, Atmos. Environ., 38, 6135-6138, 2004.

807 Väkevä, M., Kulmala, M., Stratmann, F., and Hämeri, K.: Field measurements of hygroscopic properties
808 and state of mixing of nucleation mode particles, Atmospheric Chemistry and Physics, 2, 55-66, 2002.

809 Veghte, D. P., Altaf, M. B., and Freedman, M. A.: Size dependence of the structure of organic aerosol,
810 Journal of the American Chemical Society, 135, 16046-16049, 2013.

811 Gonçalves, W. A., Machado, L. A. T., and Kirstetter, P.-E.: Influence of biomass aerosol on precipitation
812 over the Central Amazon: an observational study, Atmos. Chem. Phys., doi: 10.5194/acp-15-6789-2015,
813 2015.

814 Wang, J., Cubison, M. J., Aiken, A. C., Jimenez, J. L., and Collins, D. R.: The importance of aerosol
815 mixing state and size-resolved composition on CCN concentration and the variation of the importance
816 with atmospheric aging of aerosols, Atmospheric Chemistry and Physics, 10, 7267-7283, 2010.

817 Wang, X., Heald, C. L., Ridley, D. A., Schwarz, J. P., Spackman, J. R., Perring, A. E., Coe, H., Liu, D.,
818 and Clarke, A. D.: Exploiting simultaneous observational constraints on mass and absorption to estimate
819 the global direct radiative forcing of black carbon and brown carbon, Atmospheric Chemistry and Physics,
820 14, 10989-11010, 2014.

821 Whitehead, J. D., Darbyshire, E., Brito, J., Barbosa, H. M., Crawford, I., Stern, R., Gallagher, M. W.,
822 Kaye, P. H., Allan, J. D., and Coe, H.: Biogenic cloud nuclei in the central Amazon during the transition

from wet to dry season, Atmospheric Chemistry and Physics, 16, 9727-9743, 2016.

Wu, Z. J., Zheng, J., Shang, D. J., Du, Z. F., Wu, Y. S., Zeng, L. M., Wiedensohler, A., and Hu, M.: Particle hygroscopicity and its link to chemical composition in the urban atmosphere of Beijing, China, during summertime, Atmos. Chem. Phys., 16, 1123-1138, 2016.

Yates III, L. M., Wandruszka, R.V.: Decontamination of polluted water bytreatment with a crude humic acid blend, Environmental Science and Technology, 33, 2076-2080, 1999.

You, Y. and Bertram, A. K.: Effects of molecular weight and temperature on liquid–liquid phase separation in particles containing organic species and inorganic salts, Atmospheric Chemistry and Physics, 15, 1351-1365, 2015.

You, Y., Renbaum-Wolff, L., and Bertram, A. K.: Liquid–liquid phase separation in particles containing organics mixed with ammonium sulfate, ammonium bisulfate, ammonium nitrate or sodium chloride, Atmospheric Chemistry and Physics, 13, 11723-11734, 2013.

Yuan Youa, L. R.-W., Marc Carreras-Sospedrab, Sarah J. Hannaa, Naruki Hiranumac, Saeid Kamald,, Mackenzie L. Smithe, X. Z., Rodney J. Weberf, John E. Shillingg, Donald Dabdubb, Scot T. Martine,h,1,, and Bertrama, a. A. K.: Images reveal that atmospheric particles can undergo liquid–liquid phase separations, pnas, 109, 13188-13193, 2012.

Zamora, I. R., Tabazadeh, A., Golden, D. M., and Jacobson, M. Z.: Hygroscopic growth of common organic aerosol solutes, including humic substances, as derived from water activity measurements, Journal of Geophysical Research: Atmospheres, doi:10.1029/2011JD016067, 2011.

Zardini, A. A., Sjogren, S., Marcolli, C., Krieger, U. K., Gysel, M., Weingartner, E., Baltensperger, U., and Peter, T.: A combined particle trap/HTDMA hygroscopicity study of mixed inorganic/organic aerosol particles, Atmospheric Chemistry and Physics, 8, 5589-5601, 2008.

Zawadowicz, M., Proud, S., Seppalainen, S., and Cziczo, D.: Hygroscopic and phase separation properties of ammonium sulfate/organics/water ternary solutions, Atmospheric Chemistry and Physics, 15, 8975-8986, 2015.

Zhang, Q., Jimenez, J. L., Canagaratna, M. R., Allan, J. D., Coe, H., Ulbrich, I., Alfarra, M. R., Takami,

849 A., Middlebrook, A. M., Sun, Y. L., Dzepina, K., Dunlea, E., Docherty, K., DeCarlo, P. F., Salcedo, D.,
850 Onasch, T., Jayne, J. T., Miyoshi, T., Shimono, A., Hatakeyama, S., Takegawa, N., Kondo, Y., Schneider,
851 J., Drewnick, F., Borrmann, S., Weimer, S., Demerjian, K., Williams, P., Bower, K., Bahreini, R., Cottrell,
852 L., Griffin, R. J., Rautiainen, J., Sun, J. Y., Zhang, Y. M., and Worsnop, D. R.: Ubiquity and dominance
853 of oxygenated species in organic aerosols in anthropogenically-influenced Northern Hemisphere
854 midlatitudes, Geophysical Research Letters, doi:10.1029/2007GL029979, 2007.

855 Zhang, S. L., Ma, N., Kecorius, S., Wang, P. C., Hu, M., Wang, Z. B., Größ, J., Wu, Z. J., and
856 Wiedensohler, A.: Mixing state of atmospheric particles over the North China Plain, Atmos. Environ.,
857 125, Part A, 152-164, 2016.

858 Zhong, M. and Jang, M.: Dynamic light absorption of biomass-burning organic carbon photochemically
859 aged under natural sunlight, Atmospheric Chemistry and Physics, 14, 1517-1525, 2014.

860 Zuend, A., Marcolli, C., Booth, A. M., Lienhard, D. M., Soonsin, V., Krieger, U. K., Topping, D. O.,
861 McFiggans, G., Peter, T., and Seinfeld, J. H.: New and extended parameterization of the thermodynamic
862 model AIOMFAC: calculation of activity coefficients for organic-inorganic mixtures containing carboxyl,
863 hydroxyl, carbonyl, ether, ester, alkenyl, alkyl, and aromatic functional groups, Atmospheric Chemistry
864 and Physics, 11, 9155-9206, 2011.

865 Zuend, A., Marcolli, C., Luo, B. P., and Peter, T.: A thermodynamic model of mixed organic-inorganic
866 aerosols to predict activity coefficients, Atmospheric Chemistry and Physics, 8, 4559-4593, 2008.

867 Zuend, A., Marcolli, C., Peter, T., and Seinfeld, J. H.: Computation of liquid-liquid equilibria and phase
868 stabilities: implications for RH-dependent gas/particle partitioning of organic-inorganic aerosols,
869 Atmospheric Chemistry and Physics, 10, 7795-7820, 2010.

870 Zuend, A. and Seinfeld, J. H.: Modeling the gas-particle partitioning of secondary organic aerosol: the
871 importance of liquid-liquid phase separation, Atmospheric Chemistry and Physics, 12, 3857-3882, 2012.

872

873

874

Atmos. Chem. Phys. Discuss., https://doi.org/10.5194/acp-2017-549
Manuscript under review for journal Atmos. Chem. Phys.
Discussion started: 20 June 2017


Atmospheric Chemistry and Physics Discussions

875 **Table 1.** Substances and their physical properties used in this work.

| Chemical compound | Chemical formula | Molar Mass [g mol$^{-1}$] | Density in solid or liquid state [g cm$^{-3}$] | Solubility g/100cm$^3$ $H_2O$ | Solution surface tension [J m$^{-2}$] | Manufacturer |
|---|---|---|---|---|---|---|
| Ammonium sulfate | $(NH_4)_2SO_4$ | 132.140 | 1.770[a] (solid), 1.550[a](liquid) | 74.400(at 20℃) | 0.072(0.001-10mg/mL) | Alfa Aesar, 99.95% |
| Levoglucosan | $C_6H_{10}O_5$ | 126.100 | 1.618[b](solid) 1.512[b](liquid) | | 0.073[e] (0.01-10mg/mL) | Aldrich, 99% |
| 4-Hydroxybenzoic acid | $C_7H_6O_3$ | 138.100 | 1.460(solid) 1.372[f](liquid) | 0.675(at 25℃) | 0.070[g] (>10mg/mL) | Alfa Aesar, 99.99% |
| Humic acid | | NA | 0.800[h](solid) | NA | NA | Aldrich, 99% |

876 [a]Clegg and Wexler, (2011);
877 [b]Lienhard et al, (2012);
878 [e]Tuckermann and Cammenga (2004) at 293K;
879 [f]Jedelsky et al, (2000);
880 [g]Kiss et al, (2005);
881 [h]Yates III and Wandruszka, (1999);
882
883
884
885
886
887
888
889
890
891
892

Atmos. Chem. Phys. Discuss., https://doi.org/10.5194/acp-2017-549
Manuscript under review for journal Atmos. Chem. Phys.
Discussion started: 20 June 2017


Atmospheric Chemistry and Physics Discussions

893 **Table 2.** The chemical composition of biomass-burning model mixtures studied given as mass
894 percentages (wt %).

| Mixture name | Levoglucosan | 4-Hydroxybenzoic acid | Humic acid | Ammonium sulfate |
|---|---|---|---|---|
| Mix-bio-dry | 87.2% | 9.2% | 1.5% | 2.1% |
| Mix-bio-wet | 68.0% | 26.0% | 3.0% | 3.0% |

895
896
897
898
899
900
901
902
903
904
905
906
907
908
909
910
911

Atmos. Chem. Phys. Discuss., https://doi.org/10.5194/acp-2017-549
Manuscript under review for journal Atmos. Chem. Phys.
Discussion started: 20 June 2017


Atmospheric Chemistry and Physics Discussions

912

913 **Table 3.** Coefficients ($c_1$, $c_2$, $c_3$) of the fitted growth factor parameterization (Eq. 5) as follows:

| Chemical compounds | $c_1$ | $c_2$ | $c_3$ |
|---|---|---|---|
| Levoglucosan | 0.12868746 | 0.36582023 | -0.39840382 |
| 4-Hydroxybenzoic acid | -1.389967E-01 | 2.325586E-01 | -9.891943E-02 |
| Humic acid | -1.618304E-02 | 2.202483E-01 | 2.005134E-02 |

914

915

916

917

918

919

920

921

922

923

924

925

926

927

928

929

930

Atmos. Chem. Phys. Discuss., https://doi.org/10.5194/acp-2017-549
Manuscript under review for journal Atmos. Chem. Phys.
Discussion started: 20 June 2017


Atmospheric Chemistry and Physics Discussions

**Table 4:** Experimental studies of organic and ammonium sulfate (AS) deliquescence and efflorescence RH from this work and previous studies at 298K.

| Signal compound/Mixture | Organic mass fraction (%) | Deliquescence relative humidity of AS or organic in the mixed particle | Efflorescence relative humidity of AS or organic in the mixed particle |
|---|---|---|---|
| Levoglucosan | - | 80%[a*] | < 4%[a*] |
| | | 82.8%[b] | |
| | 25 | 80% | 45% |
| Levoglucosan+AS | 50 | - | - |
| | 75 | - | - |
| 4-hygroxybenzoic acid | - | > 97%[a*] | < 4%[a*] |
| | 25 | 80% | 35% |
| 4-Hydroxybenzoic acid+AS | 50 | 80% | 25% |
| | 75 | 80% | - |
| Humic acid | - | - | - |
| | 20 | 80% | 35% |
| Humic acid+AS | 50 | 80% | 35% |
| | 75 | 80% | 35% |

[*]is the DRH and ERH of pure organic components.

[a]Mochida and Kawamura. (2004)

[b]Zamora et al. (2011)

Atmos. Chem. Phys. Discuss., https://doi.org/10.5194/acp-2017-549
Manuscript under review for journal Atmos. Chem. Phys.
Discussion started: 20 June 2017


Atmospheric Chemistry and Physics Discussions

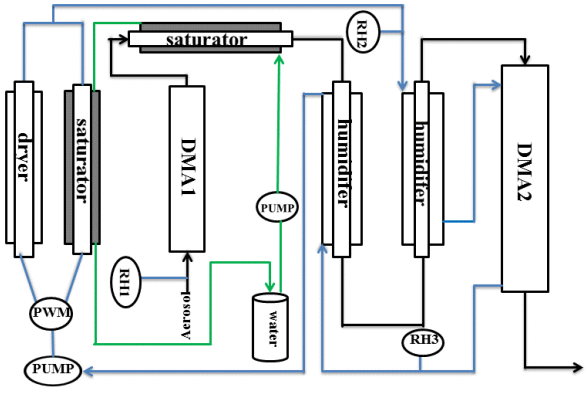


938

939 **Figure 1.** Schematic of the hygroscopicity tandem different mobility analyzer (HTDMA) system. the
940 sheath flow, aerosol flow, and water flow have been represented by the blue, black, green line,
941 respectively. PWM: Pulse Width Modulator circuit.

942

943

944

945

946

947

948

Atmos. Chem. Phys. Discuss., https://doi.org/10.5194/acp-2017-549
Manuscript under review for journal Atmos. Chem. Phys.
Discussion started: 20 June 2017


Atmospheric Chemistry and Physics Discussions

949

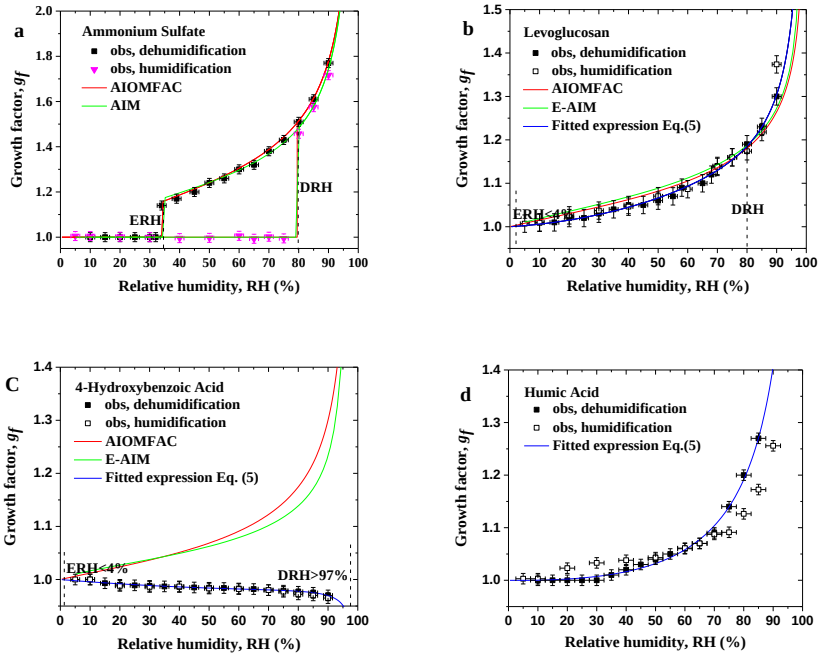


950

951 **Figure 2.** Hygroscopic growth, deliquescence and efflorescence of aerosol particles. Hygroscopic growth
952 factors of (**a**) ammonium sulfate (AS), (**b**) levoglucosan, (**c**) 4-hydroxybenzoic acid, and (**d**) humic acid
953 aerosol particles with dry diameter of 100 nm (open, black square). In this study, the green curves show
954 E-AIM predictions, and the red curves the AIOMFAC predictions, and the blue lines the fitted expression
955 (Eq. 5).

956

957

958

Atmos. Chem. Phys. Discuss., https://doi.org/10.5194/acp-2017-549
Manuscript under review for journal Atmos. Chem. Phys.
Discussion started: 20 June 2017


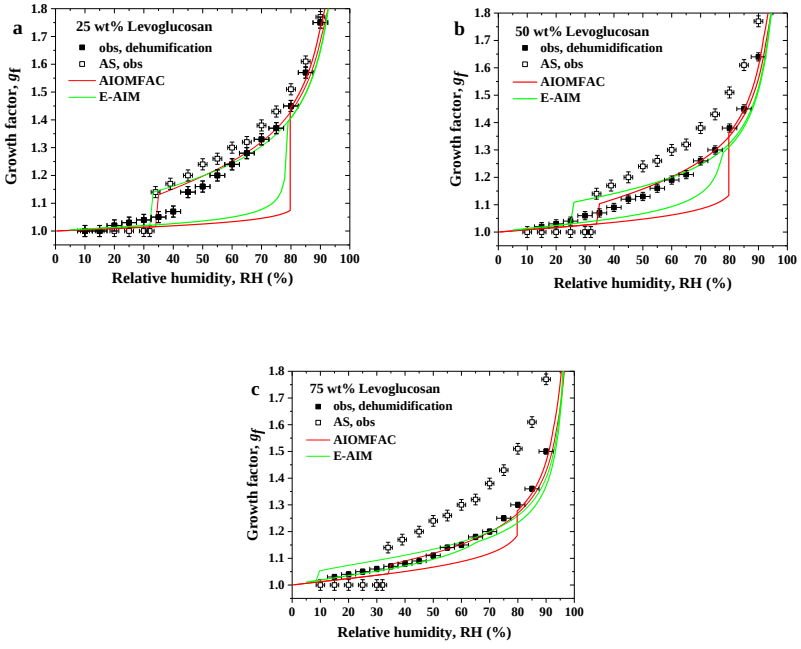


**Figure 3.** Hygroscopic growth, efflorescence of aerosol particles, and model predictions represent the diameter growth factor during dehydration experiments in the range from 90 % to 5 % RH at 298.15 K. (**a,b,c**). Hygroscopic growth curves of mixtures consisting of levoglucosan and ammonium sulfate (solid symbols) at three different dry state mass fraction for particles of an initial dry diameter of 100 nm at RH < 5 %) as compared to that of pure ammonium sulfate (open symbols, "AS, obs"). AIOMFAC-based model predictions for bulk systems are shown in red, E-AIM predictions are shown in green.

Atmos. Chem. Phys. Discuss., https://doi.org/10.5194/acp-2017-549
Manuscript under review for journal Atmos. Chem. Phys.
Discussion started: 20 June 2017


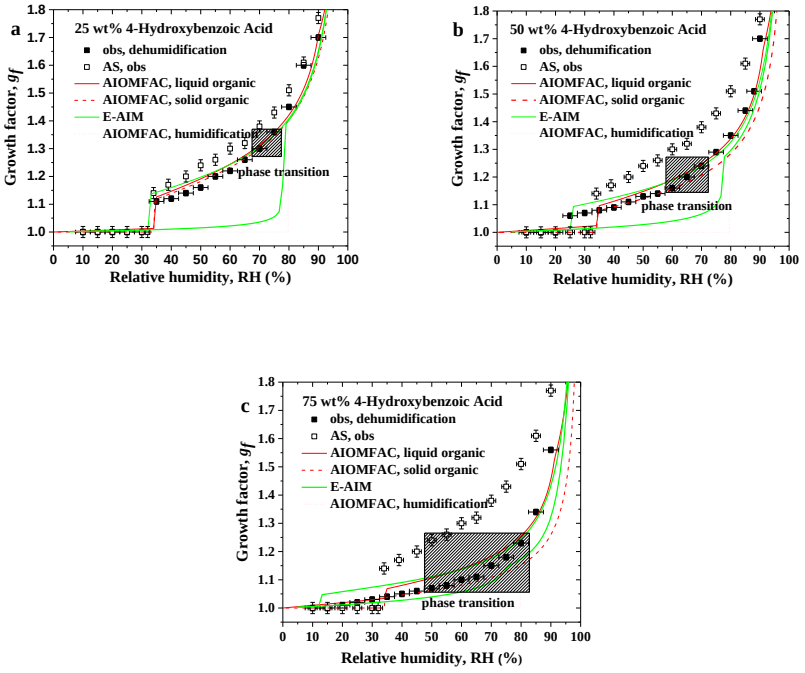


**Figure 4.** Hygroscopic growth factors, efflorescence of behavior, and model predications for dehydration experiments in the range from 90 % to 5 % RH at 298.15 K. (**a,b,c**) hygroscopic growth curves of mixtures consisting of 4-hydroxybenzoic acid and ammonium sulfate (solid symbols) at three different dry state mass fraction (initial dry diameter of 100 nm at RH < 5 % ) as compared to that of pure ammonium sulfate (open symbols). AIOMFAC-based model predictions for bulk systems are shown in red, E-AIM-predictions are shown in green for the case of assuming that 4-hydroxybenzoic acid remains. Shaded rectangle: RH range of gradual crystallization of 4-hydroxybenzoic acid.

Atmos. Chem. Phys. Discuss., https://doi.org/10.5194/acp-2017-549
Manuscript under review for journal Atmos. Chem. Phys.
Discussion started: 20 June 2017


Atmospheric Chemistry and Physics Discussions

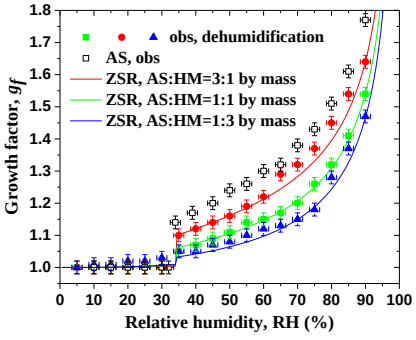


979

980 **Figure 5**. Hygroscopic growth factors, efflorescence of aerosol particles/constituents consisting of humic
981 acid and ammonium sulfate at three different dry state mass fractions with initial dry diameter of 100 nm
982 at RH < 5 % as compared to that of pure ammonium sulfate (open symbols). Colored curves: ZSR
983 predictions of dimeter growth factors for dry particle compositions corresponding to the experimental
984 data during dehumidification in the range from 90 % to 5 % RH at 298.15 K.

985

986

987

988

989

990

991

992

993

994

995

Atmos. Chem. Phys. Discuss., https://doi.org/10.5194/acp-2017-549
Manuscript under review for journal Atmos. Chem. Phys.
Discussion started: 20 June 2017


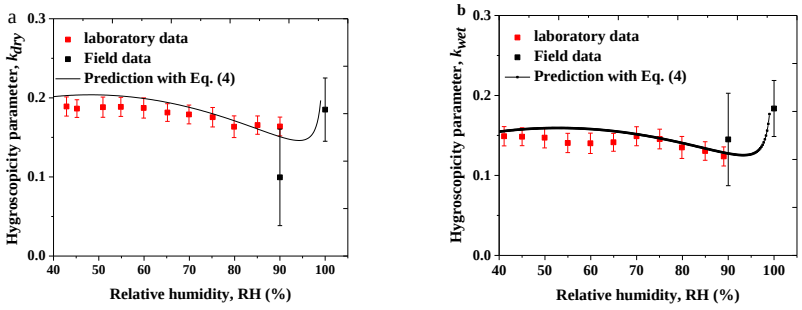


996

997 **Figure 6.** Hygroscopicity parameter, $\kappa$, representing mixed aerosol particles consisting of organic
998 surrogate components and ammonium sulfate at different periods (initial dry diameter of 100 nm at RH
999 < 5 %). The black curves in panels (a, b) show the $\kappa$ prediction from Eq. (4) with $HGF_{mix}$ calculated by
1000 Eq. (6) using component volume fractions and the HGF of the individual mixture components from a fit
1001 to the laboratory data (using Eq.5). the black symbols and error bars show field data from the Amazon
1002 during the dry and wet periods at conditions of water vapor sub-saturation (HTDMA measurement) and
1003 super-saturation ($\kappa_{CNN}$) (Whitehead et al., 2016; Pöhlker et al., 2006).

1004

1005

1006